Jour. of the KGS Vol. 17, No. 3. June 2001, pp 15~23

# A Smooth Elasto-Plastic Cap Model(I): Rate Formulation, Yield Surface Determination

## 연속 탄소성 캡 모델(I): 구성모델 및 항복면의 결정

Seo, Young-Kyo* 서 영 교


### 요 지

탄소성 캡 모델의 중요한 장점은 여러 가지 다공체의 전체적인 축차 및 체적의 비선형 상호거동을 동시에 다룰 수 있음에 있다. 그러나 대부분의 캡 모델이 가진 문제점중의 하나는 세 개의 독립적인 항복면이 불연속으로 연결되어 있음으로부터 기인된다. 본 연구에서는 이러한 항복면 사이의 연결점에서의 탄소성 접선 계수는 특이점이 되고 수치해석상 잠재적인 어려움을 내재하고 있음을 나타내고 이러한 문제의 해결방안의 하나로 세 개의 항복면이 연속적으로 만나는 새로운 탄소성 캡 모델을 제시하였다. 본 논문에서는 모델의 증분형태의 구성식 및 새로운 응력을 구하기 위한 활동 항복면의 결정을 판단하는 알고리즘이 제시되었다. 동반 논문에서는 내재적인 응력적분 및 일관적인 접선계수를 유도하였고 예제계산들을 수행하였다.

### Abstract

The primary strengths of elasto-plastic cap model are their ability to capture the gross inelastic coupling between deviatoric and volumetric behaviors of many porous media. One of the difficulties associated with most isotropic cap models is that the three independent surfaces comprising the yield surface intersect non-smoothly. It is shown here that the elasto-plastic tangent operators at the corner points on such yield surfaces are singular, giving rise to the potential numerical difficulties. To address this issue, a novel, three-surface elasto-plastic cap model in which the three surfaces intersect smoothly is developed here. In this paper, the rate form of the model constitutive equations and a detailed algorithm for active yield surface determination are presented. In the companion paper, the integration algorithms and expression for consistent tangent operators will be presented. Also, sample computations will be presented there.


**Keywords** : Cap models, Elasto-Plasticity, Finite element method, Soil Models, Computational Plasticity

## 1. Introduction

A challenging problem in computational geomechanics is the development of constitutive stress-strain models for soils that provide both physical presentation of observed mechanical behaviors and sound numerical performance in implicit computational analysis. For successful usage in implicit analysis of geomechanical structures, soil models must have numerical implementations that are also complete, stable, and continuously differentiable. Elasto-plastic soil models are a class of material models that can provide some degree of both physical realism and potentially sound numerical performance.

* Member, Fulltime Researcher, Pusan National Univ.

In 1971, DeMaggio and Sandler proposed a specific elasto-plastic cap model(as shown in Figure 1) and numerical implementation. In the family of cap models advanced by DiMaggio and Sandler, the hardening cap is an elliptical surface with a constant ratio of major to minor radius, and it intersects the failure envelope in a non-smooth fashion. The intersection point, or the so-called corner point, at which the Drucker-Prager envelope and the moving compression cap intersect, has long been recognized as the point that can give rise to both numerical and constitutive instabilities[Bathe et al(1980) and Resende & Martin(1985)]. A robust numerical implementation of cap model has been advanced by the researchers [Ortiz & Simo(1986), Simo et al(1988), and Hofstetter et al (1993)], but problems still remain in the non-smooth three-surface cap model. As will be shown below, one of the primary remaining difficulties is that the material tangent operators in both the compression corner and tension corner regions are singular in that they do not provide any bulk/volumetric material systems. While there are number of ad-hoc ways to deal with this singularity of tangent operators at the corner points (such as the introduction of artificial bulk stiffness in the corner regions, or resorting to usage of visco-plasticity as proposed in Simo et al(1988) for general non-smoothness), these approaches are less than satisfactory.

The intention of this paper is therefore, to introduce and fully develope a novel, smooth cap model wherein the three surfaces intersect in a smooth fashion such that there are no corner regions. This smoothness therefore precludes many of the historical difficulties associated with the corner regions including: material softening response, lack of completeness, and singularity of material tangent operators. The model features essentially the same physical degree of realism as the preceding cap models, but its numerical performance characteristics are significantly enhanced.

## 2. Assessment of a Non-Smooth Cap Model

### 2.1 Basic Forms and Rate Equations

For simplicity and clarity, the elasto-plastic constitutive equations of a non-smooth three surface cap model are considered here in a small deformation framework. These equations can be straightforwardly extended to a large deformation framework as necessary. The small strain tensor admits the usual additive elastic, plastic decomposition as follows:

$$\varepsilon = \varepsilon^e + \varepsilon^p \tag{1}$$

where $\varepsilon$, $\varepsilon^e$ and $\varepsilon^p$ are the total, elastic, and plastic strain tensors, respectively. The elastic response of the material is assumed to be characterized by a constant isotropic tensor $C = K\,1\otimes 1 + 2\mu\, I_{dev}$ such that the incremental stress response of the material is given by

$$\dot{\sigma} = C:(\dot{\varepsilon} - \dot{\varepsilon}^p) \tag{2}$$

In stress space, the elastic domain is bounded by three distinct yield surfaces which are functions of the two invariants $I_1 = tr(\sigma)$ and $||s||$, where $s$ is the deviatoric part of the stress tensor $\sigma$ ($i.e.$, $s = I_{dev} : \sigma$). The three surfaces comprising the yield surface intersect in a non-smooth manner as shown in Fig. 1.

The mathematical forms of the individual yield functions, $f_m(\sigma, x)$, $m = 1, 2, 3$ are

$$f_1(\sigma) = ||s||^2 - F_e^2(I_1) \le 0 \tag{3}$$

$$f_2(\sigma, x) = ||s||^2 - F_c(I_1, x) \le 0 \tag{4}$$

$$f_3(\sigma) = I_1 - T \le 0 \tag{5}$$

Specific forms for $F_e$ and $F_c$ are

$$F_e(I_1) = \alpha - \theta I_1 - \lambda \exp[\omega I_1] \tag{6}$$

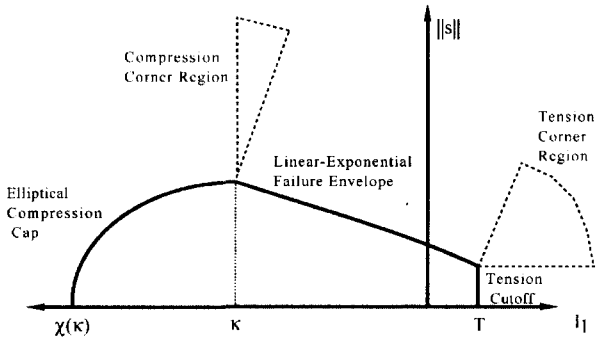


Fig. 1 Non-smooth, three surface, two-invariant cap model yield surface with two corner regions

$$F_c(I_1, x) = F_e^2(x) - \left[\frac{I_1 - x}{R}\right]^2 \tag{7}$$

where the followings are material model constants: $\alpha \geq 0$, $\lambda \geq 0$, $\omega \geq 0$, $\theta \geq 0$ and $R > 0$. The yield surfaces $f_1 = 0$ and $f_3 = 0$ depend only on the stress invarients $I_1$ and $||s||$, and thus remain fixed in stress space. In the function $F_e$, the constants $\theta$ and $\alpha$ are related, respectively, to the Mohr-Coulomb angle of friction, $\phi$ and cohesions, $c$ (Chen and Saleeb, 1982). The aspect ratio of the elliptical compression cap is provided by the dimensionless constant $R$. The cap is permitted to translate along the $I_1$ axis, and in particular moves to the right ($\dot{x} > 0$) during plastic dilatation of the medium, and to the left ($\dot{x} < 0$) during plastic compaction.

The hardening law for this model derives from the fact that the volumetric crush curve (plastic volumetric strain $\varepsilon_v^p$ versus $I_1$) is assumed to be an exponential of the form

$$\varepsilon_v^p = -W\{1 - \exp[DX(x)]\} \tag{8}$$

where $X(x) = x - RF_e(x)$ is the apex point of the cap surface on the $I_1$ axis; $\varepsilon_v^p$ denotes the plastic volumetric strain in the soil (or porous medium) as measured from a virgin completely unloaded state; $W$ represents the maximum possible plastic volumetric strain for the medium, with the reference state being the material's virgin unloaded state; and $D^{-1} = I_1^{ref}$ denotes the absolute value of $I_1$ at which $e^{-1} \cdot 100\%$ of the medium's original crushable porosity remains. Differentiating Equation (8) with respect to $x$ allows us to obtain a variable tangent hardening modulus $h'(x)$ for $x$ as following:

$$h'(x) = \frac{d\varepsilon_v^p}{dx} = \frac{\exp(-DX)}{WDX'} \tag{9}$$

where $X' = 1 - RF_e(x)$. Based on Equations (8) and (9), it is clear that as $X \to \infty$ then $h'(x) \to \infty$ and $\varepsilon_v^p \to -W$. This nonlinear hardening modulus $h'(x)$ is used to provide a nonlinear incremental hardening law governing movement of the cap parameter

$$\dot{x} = h'(x)\ tr(\dot{\varepsilon}^p) \tag{10}$$

The flow rule for this non-smooth model is associated, and since multiple surfaces are potentially active at any given instant, it takes Koiter's generalized form

$$\dot{\varepsilon}^p = \sum_m \dot{\gamma}^m \frac{\partial f_m}{\partial \sigma} \tag{11}$$

The plastic consistency parameters are denoted by $\gamma^m$ ($m = 1, 2, 3$), and their time derivatives are proportional to the instantaneous magnitudes of the plastic deformation processes at a fixed material point with respect to each of the three yield functions. Loading and unloading criteria are specified by the Karesh-Kuhn-Tucker conditions as

$$f_m \leq 0; \qquad \dot{\gamma}^m \geq 0; \qquad \dot{\gamma}^m f_{m=0} \tag{12}$$

with generalized plastic consistency expressed by

$$\dot{\gamma}^m \dot{f}_m = 0 \tag{13}$$

In accordance with the KKT conditions, this elasto-plastic constitutive model poses six different possibilities

0. The stress point $\sigma$ lies inside yield surface and $f_m < 0$. In this case the material response is incrementally elastic;
1. Loading is occurring on surface 1, such that $f_1 = 0$ and $\dot{\gamma}^1 > 0$;
2. Loading is occurring on surface 2, such that $f_2 = 0$ and $\dot{\gamma}^2 > 0$;
3. Loading is occurring on surface 3, such that $f_3 = 0$ and $\dot{\gamma}^3 > 0$;
4. Surfaces 1 and 2 are simultaneously active, such that $f_1 = f_2 = 0$ and $\dot{\gamma}^1, \dot{\gamma}^2 > 0$;
5. Surfaces 1 and 3 are simultaneously active, such that $f_1 = f_3 = 0$ and $\dot{\gamma}^1, \dot{\gamma}^3 > 0$;

In essence, this model is comprised of five elasto-plastic subcases as listed above. Those that can create some difficulty are corner Cases 4 and 5 as briefly detailed below.

## 2.2 The Problem: Singular Tangent Operators at Corner Points

To illustrate the difficulty associated with the corner cases of non-smooth cap models, the return mapping algorithm for the corner Case 4 is briefly formulated below. Upon differentiating the Case 4 stress update algorithm, it is shown that the associated consistent tangent operator obtained is singular in that it provides no volumetric stiffness for the material. This can lead to singular(rank deficient) global tangent stiffness matrix operators, and severe computational difficulties when attempting to solve global force finite element equations. While band-aid type remedies to this problem are available, the difficulty can be avoided altogether by resorting to a cap model in which the yield surfaces intersect in a smooth fashion. Such a model is introduced in the following section.

If a Backward Euler integration algorithm is applied to the elasto-plastic rate constitutive equations laid out above, then a stress update algorithm with an elastic predictor and a plastic corrector(return mapping) is the result. The elastic predictor assumes incrementally elastic behavior, and leads to a trial stress state as follows

$$\sigma^{tr}_{n+1} = \sigma_n + C : \triangle \varepsilon_{n+1} \tag{14}$$

$$\kappa^{tr}_{n+1} = \kappa_n \tag{15}$$

If the elastic predictor lies outside of the elastic domain, then one or more of the intersecting yield surfaces will be active. If it is assumed that the elastic predictor lies in the attractor region for the corner point at which the compression cap and failure envelope intersect(i.e. the compression corner region of Fig. 1) then the return map(plastic corrector) brings the stress state back to the indicated corner point. Specifically,

$$\sigma_{n+1} = \sigma^{tr}_{n+1} - K(\triangle \varepsilon^p_v)_{n+1}\, 1 - 2\mu \triangle e^p_{n+1} \tag{16}$$

where $(\varepsilon^p_v)_{n+1} = tr(\triangle \varepsilon^p_{n+1})$ is the plastic volumetric strain increment, and $\triangle e^p_{n+1} = I_{dev} : (\triangle \varepsilon^p_{n+1})$ is the deviatoric plastic strain increment. The total plastic strain increment associated with the return map is

$$\triangle \varepsilon^p_{n+1} = \hat{\gamma}^1_{n+1} \frac{\partial f_1}{\partial \sigma_{n+1}} + \hat{\gamma}^2_{n+1} \frac{\partial f_2}{\partial \sigma_{n+1}} \tag{17}$$

The magnitudes of the plastic deformation processes $\hat{\gamma}^1_{n+1}$ and $\hat{\gamma}^2_{n+1}$ are computed by enforcing $(f_1)_{n+1} = 0$ and $(f_2)_{n+1} = 0$, which provides

$$\hat{\gamma}^1_{n+1} = \frac{\kappa_n - (I^{tr}_1)_{n+1}}{9K\left(\frac{\partial F_e}{\partial I_1}\right)_{n+1}} \tag{18}$$

$$\hat{\gamma}^2_{n+1} = \frac{||s_{n+1}|| - F_e(\kappa_n)}{2\mu} - \frac{\kappa_n - (I^{tr}_1)_{n+1}}{9K\left(\frac{\partial F_e}{\partial I_1}\right)_{n+1}} \tag{19}$$

Hence the return map to the corner point is very simple and involves no iterations.

However, when one differentiates the stress increment produced by this integration algorithm with respect to the deriving strain increment, a singular consistent tangent operator is obtained. Differentiating Equation (16) and the subsidiary terms Equations (17)-(19) with respect to $\triangle \varepsilon_{n+1}$ provides the following consistent operator when surfaces 1 and 2 are simultaneously active

$$\frac{\partial \triangle \sigma_{n+1}}{\partial \triangle \varepsilon_{n+1}} = 2\mu \left[ 1 - \frac{2\mu(\hat{\gamma}^1_{n+1} + \hat{\gamma}^2_{n+1})}{||s^{tr}_{n+1}||} \right] (I_{dev} - n_{n+1} \otimes n_{n+1}) \tag{20}$$

where $n_{n+1}$ is the deviatric component of the unit normal to the yield surface at the converged stress point. Clearly, this tangent material stiffness operator has no bulk stiffness, and thus it is singular. A similar singular tangent operator with no bulk stiffness occurs at the corner point between the tension cutoff surface and the failure envelope.

According to the author's experience such singular material tangent operators can give rise to rank deficient global tangent stiffness matrices when implicit nonlinear finite element calculations are performed with non-smooth cap models. There are a number of band-aid type solutions that can be employed to deal with this problem. Two in particular are:

1. Introduction of an artificial (and small) bulk stiffness to the material tangent defined in Equation (20)
2. Introduction of visco-plasticity to the model, which

allows the tangent operators in corner regions to remain non-singular as long as the inviscid limit is not approached.

Neither of these band-aid type approaches deals with the root cause of the problem, however, which is the existence of corner points on the yield surface. Furthermore, the introduction of the artificial bulk stiffness in the corner regions can lead to a tangent operator that is inconsistent with the stress update algorithm, and thus result in slow convergence behavior in solving nonlinear global force balance equations. The introduction of viscoplastic behaviors to avoid singularity of tangent operators in the corner regions makes the structural analysis problem somewhat more involved, since for each structural load increment applied, a number of time steps must be permitted to compute the time dependent deformation response of the structure. Furthermore, the rate dependence introduced with viscoplasticity can obscure more physically based rate effects such as those associated with pore pressure diffusion phenomena. A more fundamental approach to this problem of singular tangent operators in corner regions is therefore proposed as below, with the introduction of a smooth cap model having no corner regions.

## 3. Introduction of a Novel Smooth Cap Model

### 3.1 Basic Forms and Rate Equations

To deal with the difficulties associated with a non-smooth yield surface, a yield surface (as shown in Fig. 2) made up of three smoothly intersecting yield functions is introduced here. The forms of the yield function, $f_m(\sigma, x)$ $(m=1,2,3)$ are specified in terms of functions $F_e$, $F_c$, and $F_t$ which are respectively called the Drucker-Prager envelope function, the compression cap function, and the tension cap function. The mathematical forms are

$$f_1(\sigma,q)=||\eta||-F_e(I_1) \le 0 \tag{21}$$

$$f_2(\sigma,q,x)=||\eta||^2-F_c(I_1,x) \le 0 \tag{22}$$

$$f_3(\sigma,q)=||\eta||^2-F_t(I_1) \le 0 \tag{23}$$

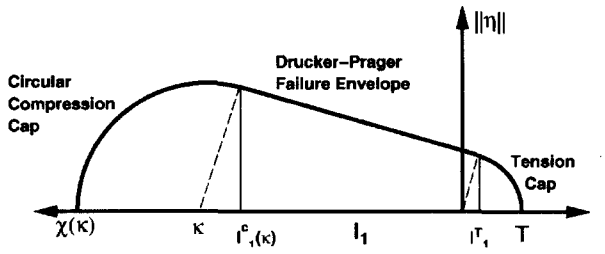


Fig. 2 Smooth, three-surface, two invariant yield function for cap

where: $\eta=s-q$ and $||\eta||^2=[\eta:\eta]^{1/2}$. As is customary $s$ denotes the deviatoric stress, and $q$ denotes a purely deviatoric back stress associated with kinematic hardening. The specific forms of $F_e$, $F_c$, and $F_t$ differ somewhat from the forms introduced previously in concert with the non-smooth cap model, and are defined here as

$$F_e(I_1)=\alpha-\theta I_1 \qquad I_1^C(x) \le I_1 \le I_1^T \tag{24}$$

$$F_c(I_1,x)=R^2(x)-(I_1-x)^2 \qquad I_1 < I_1^C(x) \tag{25}$$

$$F_t(I_1)=R_T^2-I_1^2 \qquad I_1 > I_1^T \tag{26}$$

In the preceding expressions, the entities $I_1^T$ and $I_1^C(x)$ denote, respectively, a fixed delimiting point between the Drucker-Prager envelope and the tension cap, and the Drucker-Prager envelope and the compression cap. Specific expressions for these points are

$$I_1^T=\alpha\cos(\phi)\sin(\phi) \tag{27a}$$

$$I_1^C=x+R(x)\sin(\phi) \tag{27b}$$

where $\phi=\tan^{-1}(\theta)$. As the compression cap surface translates along the $I_1$ axis, the cap surface radius $R(x)$ changes as a function of the cap parameter $x$ as follows

$$R(x)=-x\sin(\phi)+\alpha\cos(\phi) \tag{28}$$

The primary differences between the yield functions for the smooth cap model and those for the non-smooth cap models are

1. The compression cap surface is no longer elliptical, but rather strictly circular in the $||\eta||$ and $I_1$ space representation. As in the non-smooth model, the cap surface can translate left(outward) on the $I_1$ axis with plastic compression of the medium, and right

(inward) on the $I_1$ axis with plastic dilatation.

2. The circular compression cap surface is centered along the $I_1$ axis at $I_1 = x$.
3. The radius $R(x)$ of the compression cap is such that it maintains smooth tangency with the failure envelop. Hence, the radius $R(x)$ is the minimal distance from the current centerpoint $(x, 0)$ of the compression cap, to the failure envelope surface $f_2 = 0$.
4. The tension surface is no longer a planar cutoff but rather circular cap. The center of the tension cap resides at $I_1 = 0$, and the radius of the surface is a constant $T$ which is determined based on $\alpha$ and $\theta$.
5. The model features kinematic hardening which permits the elastic domain to translate about hydrostatic stress axis.

The flow rule for this model is associated as following:

$$\dot{\varepsilon}^p = \sum_m \dot{\gamma}^m \frac{\partial f_m}{\partial \sigma} \tag{29}$$

While this generalized form of the flow rule would appear to imply that more than one yield function can be active at a given instant, this will not occur with this model due to the smoothness of the yield surface of the cap model. The Karesh-Kuhn-Tucker loading/unloading conditions and the plastic consistency conditions for the smooth model are expressed in a manner identical to that for the non-smooth cap model in equations (12) and (13). In rate form, the non-associated hardening law for the cap parameter $x$ is identical to that used for non-smooth cap model shown in the equations (9) and (10). The maximum value the cap parameter $x$ can take is limited to 0, such that $x = \min\{0, x\}$. A purely deviatoric linear kinematic hardening law is employed with this model, the rate form of which is

$$\dot{q} = H\, I_{dev} \cdot \dot{\varepsilon}^p \tag{30}$$

where $H$ is a constant plastic hardening modulus.

### 3.2 Active Yield Surface Determination

The basic problem of integrating the elasto-plastic constitutive equations at a fixed material point can be stated as follows. On the time interval of interest $[0, T]$, it is assumed that at time $t_n \in [0, T]$ the total and plastic strain tensors are known as are the stress and hardening variables: which means that $\{\varepsilon_n, \varepsilon_n^p, \sigma_n, x_n, q_n\}$ are known at time $t_n$. The incremental strain $\triangle\varepsilon_{n+1}$ over a given time step $[t_n, t_{n+1}]$, is assumed to be provided, and the remaining independent variables $\{\varepsilon_{n+1}^p, \sigma_{n+1}, x_{n+1}, q_{n+1}\}$ must be updated by the integration of the rate constitutive equations. This is accomplished here using well-established operator-splitting, elasto-predictor, and plastic-corrector methods. Briefly, the updated stress can be written as follows:

$$\begin{aligned}\sigma_{n+1} &= \sigma_n + C : \triangle\varepsilon_{n+1}^e \\ &= \sigma_n + C : \triangle\varepsilon_{n+1} - C : \triangle\varepsilon_{n+1}^p\end{aligned} \tag{31}$$

In accordance with the operator-split, a given strain increment $\triangle\varepsilon_{n+1}$ is first assumed to result in an incremental material response which is fully elastic, leading to a the so-called incrementally elastic trial stress predictor computed as

$$\sigma_{n+1}^{tr} = \sigma_n + C : \triangle\varepsilon_{n+1} \tag{32a}$$

$$= \sigma_n + K\triangle\varepsilon_{n+1}^v\, 1 + 2\mu\triangle e_{n+1} \tag{32b}$$

where $\triangle\varepsilon_{n+1}^v$ is the incremental volumetric strain, and $\triangle e_{n+1}$ is the incremental deviatoric strain. Taking the trace and deviatoric parts of the elastic trial stress leads to

$$(I_1)_{n+1}^{tr} = (I_1)_n + 9K\triangle\varepsilon_{n+1}^v \tag{33a}$$

$$s_{n+1}^{tr} = s_n + 2\mu I_{dev}\triangle\varepsilon_{n+1} \tag{33b}$$

Also, the trial value of the cap hardening parameter $x$ and the back stress $q$ remain unchanged during the elastic predictor so that $x_{n+1}^{tr} = x_n$ and $q_{n+1}^{tr} = q_n$. The trial yield function values $(f_1)_{n+1}^{tr}$, $(f_2)_{n+1}^{tr}$, and $(f_3)_{n+1}^{tr}$ are then computed based on the trial stress and hardening parameters. If $(f_1)_{n+1}^{tr} > \mathrm{TOL}_1$ or $(f_2)_{n+1}^{tr} > \mathrm{TOL}_2$ or $(f_3)_{n+1}^{tr} > \mathrm{TOL}_3$, then the predicted elastic trial state lies outside the elastic domain, and a plastic correction must be performed.

Table 1. Determination of yield surface activity

Compute elastic predictor stress $\sigma_{n+1}^{tr}$ and hardening variables $q_{n+1}, \alpha_{n+1}^{tr}$

Compute yield function values $f_1^{tr}, f_2^{tr}, f_3^{tr}$ based on $\sigma_{n+1}^{tr}, q_{n+1}$ and $\alpha_{n+1}^{tr}$

IF ( $f_1^{tr} > \text{TOL}_1$ )

  Perform Case 1 return map

  Compute $(I_1)_{n+1}^{case1}$ and $\alpha_{n+1}^{case1}$

  IF ( $(I_1)_{n+1}^{case1} < I_1^C(\alpha_{n+1}^{case1})$ ) then Case 2 is active

    goto Case 2

  Elseif ( $(I_1)_{n+1}^{case1} > I_1^T$ ) then Case 3 is active

    goto Case 3

  Else

    Case 1 active

  Endif

Else

  IF ( $f_2^{tr} > \text{TOL}_2$ and $I_1^{tr} < I_1^C(\alpha_{n+1}^{tr})$ )

    goto Case 2

  Elseif ( $f_3^{tr} > \text{TOL}_3$ and $I_1^{tr} > I_1^T$ )

    goto Case 3

  Else

    Elastic predictor lies in elastic domain

  Endif

Endif

The manner in which the plastic correction is computed depends upon which one of the yield constraints is in fact active. For the general case of non-smooth plasticity models, determination of the so-called active set of yield constraints can be a challenging task as demonstrated by Simo et al(1988). Even for this smooth plasticity model, great caution is needed in determining which, if any, of the three yield constraints will be active at any given instant. The algorithm used for determining yield function activity with the proposed smooth cap model is shown in Table 1. The underlying concept for the algorithm of Table 1 is that since the Drucker-Prager surface envelopes both the tension and compression cap surfaces, when it is violated, then the second and third yield criteria will necessarily be violated as well. Thus, when $(f_1)_{n+1}^{tr} > \text{TOL}_1$, any of the three yield surfaces could in fact be active. Ultimately, however, only one will indeed be active. If the returned stress point lies in the updated domain of the Drucker-Prager surface, then that constraint will indeed be active. However, if the return point should lie in the updated domain of either the compression cap or the tension cap, they would represent the active constraint. These ideas are demonstrated graphically in Fig. 3. Referring specifically to Fig. 3b, if $(I_1)_{n+1}^{case1} > I_1^T$, then the return point lies in the domain of the tension cap surface, and so the tension cap surface will be active, which means that the return map must be re-computed using the Case 3 integration algorithm. To determine whether or not the compression cap is active, then (correponding to Fig. 3c) a value of $I_1^C(\alpha_{n+1})$ is computed which provides a delimiting point between the Drucker-Prager envelope and the circular compression cap surface. If $(I_1)_{n+1}^{case1} < I_1^C(\alpha_{n+1})$, then the compression

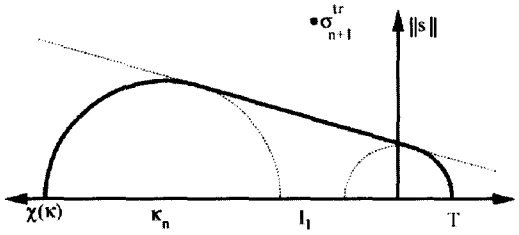


(a) Trial stress point that violates $f_1 \leq 0$ and thus violates $f_2 \leq 0$ and $f_3 \leq 0$

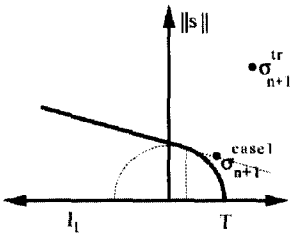


(b) Case 1 return point to the Drucker-Prager surface but lying in the tension domain

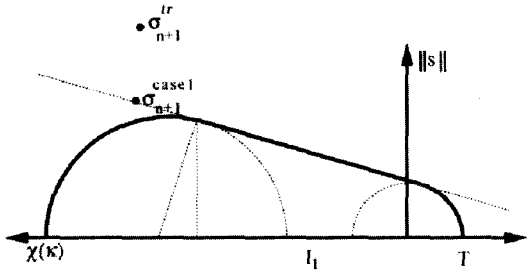


(c) Case 1 return point to the Drucker-Prager surface lying in the compression cap domain

Fig. 3 Active yield surface determination associated with $f_1^{tr} \leq$ TOL$_1$

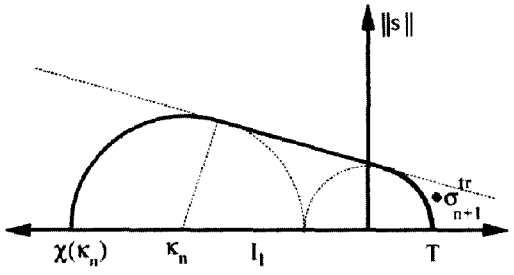


(a) Trial stress point that violates $f_2 \leq 0$ and lies in compression cap surface

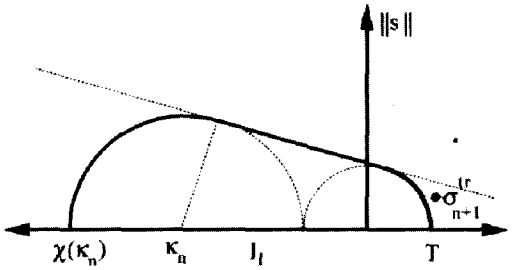


(b) Trial stress point that violates $f_3 \leq 0$ and lies in the domain of the tension cap

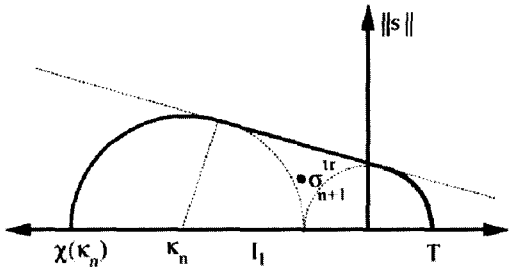


(c) Trial stress point that violates $f_2 \leq 0$ and $f_3 \leq 0$ and still lies in the elastec domain

Fig. 4 Active yield surface determination associated with $f_1^{tr} >$ TOL$_1$

cap is active and the return map must be re-computed using the Case 2 integration algorithm. It should be further noted, corresponding to Fig. 4, that it is possible for the elastic trial stress state $\sigma^{tr}_{n+1}$ to violate either or both of $f_2 \leq 0$ and $f_3 \leq 0$ but not violate $f_1 \leq 0$. In this case, it must be determined wether Case 2 or Case 3 is active.

## 4. Summary and Closure

The cap models have an elliptical yield surface and they intersect the failure envelope in a non-smooth fashion. The intersection point, so-called corner point can give rise to both numerical and constitutive instabilities. It is shown that the tangent operators in both the compression corner and tension corner regions are singular. To address this issue, a novel, three-surface elasto-plastic cap model in which the three surfaces intersect smoothly was introduced. In this paper the rate form of smooth cap model was first presented. Then the active yield surface was determined from the updated stress state due to the smoothness of the yield surfaces. In the companion paper, the specific integration algorithm and the associated consistent tangent operators will be derived for the three subcases of the model. Also sample examples will be presented for the performance of the model. This smooth

cap model features essentially the same physical degree of realism as the preceding cap models, but its numerical performance characteristics are significantly enhanced.

## References


1. Bathe, K. J., Snyder, M. D., Cimento, A. P. and Rolph, W. D. (1980), "On some current procedures and difficulties in finite element analysis of elasto-plastic response", Computers & Structures, 12, pp. 607-624.
2. Chen, W-F and saleeb, A. F. (1982), "Constitutive Equations for Engineering Materials, Vol. 1: Elasticity and Modeling", John-Wiley.
3. DiMaggio, F. L. and Sandler, I. S. (1971), "Material models for granlur soils", J. of Eng. Mech., ASCE, Vol 97, No. EM3 June, pp. 935-950.
4. Hofstetter, G., Simo, J. C. and Taylor, R. L. (1993) "A modified cap model: closest point solution algorithms", Computers & Structures, 48-2, pp. 203-214.
5. Ortiz, M. and Simo, J. C. (1986), "Analaysis of new class of integration algorithm for elasto-plastic constitutive relations", Int'l J. Numer. Meth. Eng., 23, pp. 353-366.
6. Resende, L. and Martin, J. B. (1985), "Formulation of Drucker-Prager cap model" J. Eng. Mech., 111, No. 7, pp. 855-881.
7. Simo, J. C., Ju, J-K, Pister, K. S. and Taylor, R. L. (1988), "Assessment of cap model: consistent return algorithms and rate-dependent extension", J. Eng. Meth., 114, pp. 191-218.
8. Simo, J. C., Kennedy, J. G. and Govindjee, S. (1988) "Loading/unloading conditions and numerical algorithms", Int'l J. Numer. Meth. Eng., 25, pp. 2161-2185.


(received on Mar. 22, 2001)